

Optical Spectroscopy of Galactic Cirrus Clouds¹: Extended Red Emission in the Diffuse Interstellar Medium

Arpad Szomoru
and

Puragra Guhathakurta²
UCO/Lick Observatory, University of California, Santa Cruz, California 95064

ABSTRACT

We present initial results from the first optical spectroscopic survey of high latitude Galactic cirrus clouds. The observed shape of the cirrus spectrum does not agree with that of scattered ambient Galactic starlight. This mismatch can be explained by the presence of Extended Red Emission (ERE) in the diffuse interstellar medium, as found in many other astronomical objects, probably caused by photoluminescence of hydrocarbons. The integrated ERE intensity, $I_{\text{ERE}} \approx 1.2 \times 10^{-5} \text{ erg s}^{-1} \text{ cm}^{-2} \text{ sr}^{-1}$, is roughly a third of the scattered light intensity, consistent with recent color measurements of diffuse Galactic light. The peak of the cirrus ERE ($\lambda_0 \sim 6000 \text{ \AA}$) is shifted towards short (bluer) wavelengths compared to the ERE in sources excited by intense ultraviolet radiation, such as HII regions ($\lambda_0 \sim 8000 \text{ \AA}$); such a trend is seen in laboratory experiments on hydrogenated amorphous carbon films.

Subject headings: Galaxy: solar neighborhood–ISM: clouds–ISM: dust, extinction–ISM: molecules–ISM: reflection nebulae

¹Observations carried out at the University of California's Lick Observatory, Mount Hamilton, California

²Alfred P. Sloan Research Fellow

1. Introduction

A diffuse component to the Galactic interstellar medium (ISM) was noticed over forty years ago (de Vaucouleurs 1955, 1960) in the form of scattered starlight from dust clouds (Sandage 1976). It was the IRAS all-sky survey though that first revealed cirrus as a ubiquitous component of the far-infrared sky (Low et al. 1984), demonstrating that these tenuous clouds of warm dust are representative of the diffuse ISM in our Galaxy (Beichman 1987; Boulanger 1994) and probably in all late-type spirals. Low et al. (1984) noted the positional correlation of the cirrus emission with HI clouds mapped by Heiles (1975); later optical studies of cirrus (de Vries & le Poole 1985; Paley 1990; Stark 1993) revealed a good correspondence between optical and infrared cirrus.

Since the IRAS mission, analyses of the cirrus have shown that the far-infrared emission from high latitude cirrus arises from an ensemble of silicate and graphite dust grains and complex molecules heated by the ambient interstellar radiation field (ISRF) (Low et al. 1984; Mezger et al. 1982). The color temperature of the cirrus emission at 12 and 25 μm , where visible, indicates thermal fluctuations of very small grains and/or polycyclic aromatic hydrocarbons (PAHs) within clouds (cf. Puget et al. 1985; Boulanger et al. 1985, 1988; Heiles et al. 1988; Guhathakurta & Draine 1989). There is at least an order of magnitude variation in the infrared colors from cloud to cloud, indicating considerable compositional variation.

In addition to scattered and thermally reprocessed radiation, Extended Red Emission (ERE), a broad emission feature of $\sim 1000 \text{ \AA}$ width centered between 6000 \AA and 8000 \AA , has been detected in the spectra of a wide variety of Galactic objects: reflection nebulae (Schmidt et al. 1980; Witt & Schild 1988), a high latitude Galactic dark cloud (Mattila 1979; Chlewicki & Laureijs 1987), planetary nebulae (PN) (Furton & Witt 1990, 1992), HII regions (Perrin & Sivan 1992; Sivan & Perrin 1993), and a nova (Scott et al. 1994). Recently, ERE has also been detected outside the Galaxy, in the halo of M82 (Perrin et al. 1995).

Possible carriers of the ERE include hydrogenated amorphous carbon (HAC—Duley 1985; Duley & Williams 1988, 1990), PAHs (d’Hendecourt et al. 1986), and C_{60} (Webster 1993). There is no obvious “best” candidate. PAHs have been identified with the so-called unidentified infrared emission (UIR) fea-

tures and indeed, in the reflection nebula NGC 2023, emission at 3.3 μm is correlated spatially with ERE (Burton et al. 1988; Witt & Malin 1989). However, Perrin & Sivan (1992) do not find such a correlation in the Orion nebula; moreover, 3.3 μm emission has been detected in PN with no ERE (Furton & Witt 1992). Laboratory spectra of C_{60} compare well with the observed ERE in the PN NGC 2327 (Webster 1993). The peak and shape of the ERE feature though vary for different objects, and it is unclear whether C_{60} can reproduce this variability. Whether ERE is present in all dust or only in discrete dusty objects remains, to some degree, an open question. The study of ERE in the warm diffuse ISM has important implications for the chemistry of and energy balance in this phase.

There is indirect evidence of ERE in the Galaxy’s warm diffuse interstellar medium. Unusually red broadband colors ($B - R$, $R - I$) have been measured for cirrus clouds (Guhathakurta & Tyson 1989; Paley et al. 1991; Guhathakurta & Cutri 1994), suggesting the presence of an additional component (over scattered light) in the R - and I -bands. Recent work by Gordon et al. (1997) reached a similar conclusion using a very different technique: they decomposed Pioneer 10 & 11 blue and red surface brightness maps into contributions of Galactic starlight and diffuse Galactic light. The advantage of this approach is the wide field of view, while the obvious disadvantage is poor angular resolution. All of these studies lack the spectral resolution needed to make an unambiguous detection of the ERE bump. Their interpretation is further complicated by the lack of detailed knowledge of the color of incident starlight and the amount of internal reddening within clouds.

This paper presents the first direct spectroscopy of diffuse, high latitude cirrus clouds illuminated by ambient Galactic starlight. The targets of study have low optical surface brightness, only $\sim 1\%$ of the night sky brightness (they are not bright enough to be classified as reflection nebulae), but the experiment is made possible by the availability of high efficiency modern spectrographs. These cirrus clouds have optical depths substantially below unity (typically a few tenths) making them qualitatively different from the previously studied dark cloud, L1780 (Mattila 1979), with $A_B \sim 2\text{--}5$ mag. Our spectroscopic survey covers the relatively tenuous outer edges of cirrus clouds, but even their densest central portions show none of the usual signs of high opacity: reduced surface density of background stars or increased IRAS 100 $\mu\text{m}/60 \mu\text{m}$

ratio. Sec. 2 contains a description of the observations and data reduction techniques. In Sec. 3, the spectra are analyzed in the context of scattering of starlight and photoluminescence from hydrocarbons. The main findings of this paper are summarized in Sec. 4.

2. Observations & Data Reduction

Our targets of study are compact, relatively isolated, high latitude cirrus clouds selected from IRAS $100\mu\text{m}$ maps or drawn from the catalog of Lynds Bright Nebulae (Lynds 1965) which is, in turn, derived from POSS plates. Clouds with sharp edges are ideal for making (differential) measurements of clouds relative to the adjacent sky background. The Lick Observatory Shane 3-meter telescope and KAST spectrograph were used to observe three cirrus clouds – Witch ($10^{\text{h}}44^{\text{m}}42^{\text{s}}$, $+83^{\circ}43'7''$), LBN 8 ($15^{\text{h}}50^{\text{m}}3^{\text{s}}$, $-5^{\circ}50'2''$), and Draco ($16^{\text{h}}47^{\text{m}}34^{\text{s}}$, $+60^{\circ}17'0''$) – during 2 nights in April 1997. The KAST spectrograph’s 300 lines mm^{-1} grating and Reticon 1200×400 CCD (of which 1200×200 are read out) yield a wavelength range of $\Delta\lambda = 4090\text{Å} - 9590\text{Å}$ at a dispersion of 4.6Å pixel^{-1} with $27\mu\text{m}$ pixels and a scale of about $0''.8\text{ pixel}^{-1}$. The slit width and length of $3''\times145''$ result in an overall resolution of 18.4Å (FWHM). The observations consist of 20 min exposures \times 15 pointings for the Witch and 7 pointings for each of LBN 8 and Draco, with each pointing chosen to have the slit straddle a sharp edge in the cirrus. Dome flat spectra were obtained after every change of pointing and/or of slit position angle. The spectrophotometric standard stars Feige 34 and Feige 98 were observed several times during the observing run. Observing conditions were initially photometric but degraded during the course of the first night; the second night was not photometric. The seeing FWHM was $\sim 2''$ during the observations.

As both zero level and dark current are negligible, we do not apply any overscan, bias, or dark current subtractions. For each spectrum, a flat-field image is constructed by averaging the best matched dome flats (nearest in terms of telescope pointing and slit position angle). Due to flexure of the instrument however, the fringe patterns in spectra and flat fields do not correspond exactly. To correct for this effect, we allow for a small shift of the flat fields along the dispersion axis. The optimal shift, typically $\sim 1\text{--}2$ pixels, is determined by minimizing the rms brightness varia-

tion along the slit of several bright night sky emission lines in the flat-fielded images. The spectra are then corrected for geometric distortion in the spectrograph optics by rectifying the night sky lines.

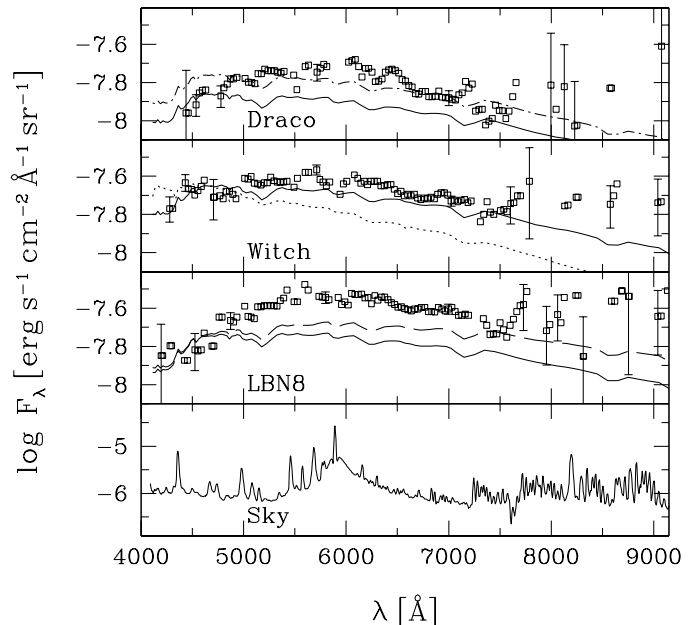


Fig. 1.— Spectra of three cirrus clouds, in order of decreasing surface brightness. Representative error bars are shown, spanning the smallest and largest errors at the blue and red ends of the spectrum. The solid lines are scattered synthetic E-type galaxy spectra (Poggianti 1997) normalized to the cirrus spectra at $\sim 4500\text{Å}$. Normalizing the scattered light model at 5000Å (dot-dashed line in first panel) reduces the inferred amount of ERE but results in a deficit for $\lambda < 4800\text{Å}$; the dotted line in the second panel is based on an Sc-type ambient spectrum; the long-dashed line in the third panel corresponds to twice the nominal optical depth. The lowest panel shows the night sky spectrum.

The low surface brightness of the cirrus ($B \sim 26\text{ mag arcsec}^{-2}$, $R \sim 24\text{ mag arcsec}^{-2}$) makes this a challenging project, and requires very accurate subtraction of the night sky spectrum, especially its bright emission lines. For a few of the spectra the task is facilitated by the fact that the long slit extends to cirrus-free parts of the sky on both sides of the cloud. The other cases are more complicated, and we use a multi-step iterative process: [1] A rel-

atively emission line free part of the night sky spectrum (6350 Å–7515 Å) is collapsed in the dispersion direction (combining several columns) to determine the exact location of the cirrus edge ($l_{\text{edge}} \approx 0.5 l_{\text{max}}$), and the brightness profile of the cirrus along the slit length, $I(l)$. [2] The cirrus free section $[0, l_{\text{edge}}]$ is used to make a preliminary measurement of the sky spectrum, which is then subtracted from each row of the full 2D spectrum. [3] This extrapolation of the night sky spectrum beyond $l > l_{\text{edge}}$ has large uncertainties, however, primarily because of imperfect rectification. We isolate a small ($\Delta l \sim 10''$) section of the (preliminary) sky-subtracted spectrum at the end of the slit opposite the cirrus-free end, $[0.9 l_{\text{max}}, l_{\text{max}}]$, and make a low-order polynomial fit, $I_{\text{fit}}^{\text{cirr}}$, to the cirrus spectrum (relying on the assumption that it is fairly smooth in λ). [4] This smooth fit, $I_{\text{fit}}^{\text{cirr}}$, is used to subtract off the contribution of the cirrus from the $[0.9 l_{\text{max}}, l_{\text{max}}]$ section of the “original” 2D spectrum (i.e., the pre-sky subtraction, flat-fielded and rectified spectrum). The final night sky spectrum is then interpolated from two extreme sections of this residual 2D spectrum: $[0, l_{\text{edge}}]$ and $[0.9 l_{\text{max}}, l_{\text{max}}]$. This final night sky spectrum is subtracted from each row of the 2D spectrum.

Next, each sky-subtracted spectrum is collapsed into a median cirrus spectrum over the appropriate section of the slit length: $[l_{\text{edge}}, 0.9 l_{\text{max}}]$. Median spectra from individual exposures of a given cloud are then combined using a noise-weighted average, with the noise determined over the “line-free” 6350 Å–7515 Å range. The rms scatter in each λ pixel amongst individual spectra is used to mask poorly subtracted night sky emission lines, especially at the red end where residual fringes are a problem. The resulting masked spectrum is then boxcar-smoothed in λ , ignoring masked pixels, to a resolution of 97 Å in order to enhance the signal-to-noise ratio.

Wavelength calibration is done using night sky lines (Osterbrock & Martel 1992) in a star- and cirrus-free part of one of the spectra. Initial flux calibration is based on observations of the Feige 34 spectrophotometric standard star. Second order overlap, combined with the high flux of Feige 34 for $\lambda \leq 4000$ Å, leads to calibration errors for $\lambda \geq 7500$ Å. To correct this, we use the initially calibrated spectra of a number of field stars that the long slit happened to intersect. Most of these stars are easily identifiable as K and M dwarfs, as their observed spectra closely resemble empirical stellar library spectra (Fioc &

Rocca-Volmerange 1997) for $\lambda \leq 7500$ Å. This enables us to determine a residual flux calibration correction for $\lambda \geq 7500$ Å (averaged over all the field stars) which is then applied to the cirrus spectra.

3. Evidence for Extended Red Emission

Figure 1 shows the calibrated spectra of all three cirrus clouds. We also plot a night sky spectrum to illustrate the strength of the night sky lines, particularly for $\lambda > 7500$ Å. Since no particularly bright star is seen in the vicinity of the clouds, it is reasonable to assume that the cirrus is illuminated by ambient Galactic starlight. This assumption is justified because: (1) the spectral shapes of clouds in different locations are roughly similar, and (2) our measurement represents an average over multiple slit positions within each cloud, effectively averaging out the illumination effects of individual bright stars.

We compare the observed spectral shape of the cirrus to a simple scattering model. The spectrum of the incident radiation field is represented by synthetic galactic spectra of various Hubble types (Poggianti 1997). The optical depth estimate is based on a standard conversion from IRAS 100 μm brightness (Savage & Mathis 1979; Boulanger & Perault 1988): $A_V = 0.053 (S_{100}/1 \text{ MJy sr}^{-1})$. This yields values of $A_V = 0.27$ for the Witch and Draco and $A_V = 0.64$ for LBN 8. In Fig. 1 we also plot the scattered starlight model normalized to the cirrus emission at ~ 4500 Å, based on an incident E-type galaxy spectrum. The grain albedo is taken to be constant in λ at $\omega = 0.55$ (Draine & Lee 1984), while the extinction law of Cardelli et al. (1989) is adopted.

It is clear that the overall *shape* of the cirrus spectrum is not fit by scattered starlight alone. In particular, the cirrus spectra have too much tilt/curvature in the region 4000 Å–7000 Å to be fit by any plausible mix of stars (spectra of galaxy types later than E produce even worse fits). Scaling the model spectrum to match the red part of the cirrus spectrum ($\lambda \gtrsim 5000$ Å) results in a deficit for $\lambda \lesssim 4800$ Å (cf. top panel of Fig. 1); we have instead chosen to scale the model spectrum to the blue side of the cirrus as the resulting broad region with excess emission (ERE) has a natural explanation. It is not quite clear whether this excess emission extends beyond $\lambda \sim 7500$ Å where measurement/calibration uncertainties are large. Incidentally, the shape of the cirrus spectrum agrees with previous broadband obser-

vations of cirrus clouds (cf. Guhathakurta & Tyson 1989), which showed both $B - R$ and $R - I$ colors to be too red to be explained by scattered Galactic light.

Note, the S_{100} values adopted are conservative in that they have not had any large scale background subtracted (due to foreground zodiacal light, for example); for LBN 8 in particular, the actual brightness of the cloud, and the inferred A_V , could be as much as a factor of 2 lower. The conversion factor of 0.053 used to derive A_V from S_{100} is well within the range found by Stark (1995) for Galactic dust clouds, based on photometry and counts of background stars. As an extreme example, we adopt a conversion factor of 0.1 for the densest cloud in our sample, LBN 8. The resulting scattered light spectrum (long-dashed line in third panel of Fig. 1) is understandably somewhat (internally) reddened relative to that derived using the nominal optical depth (solid line), but the conclusions about ERE in the cirrus are essentially unchanged. The effect of doubling the nominal optical depth is negligible for the other two clouds. Multiple scattering is ignored because $\tau_V^{\text{sca}} < 0.6$ even for the densest cloud (LBN 8) using an extreme $S_{100} \rightarrow A_V$ conversion ratio, whereas such events are only important if $\tau^{\text{sca}} > 1$.

We also check whether the observed flux density of the cirrus is consistent with an independent estimate of the strength of the ISRF in the solar neighborhood (Mathis et al. (1983): $4\pi J_\lambda(7000 \text{ \AA}) = 1.5$ and $3.1 \text{ erg s}^{-1} \text{ cm}^{-2} \mu\text{m}^{-1}$, at galactocentric distances of 10 and 8 kpc, respectively. Applying the above dust scattering parameters to the actual cirrus spectra we derive values for the incident ISRF of $1\text{--}2 \text{ erg s}^{-1} \text{ cm}^{-2} \mu\text{m}^{-1}$. The agreement with Mathis et al.’s estimate is remarkable when one considers that: (1) it is difficult to measure the effective optical depth of the cirrus averaged over the exact area represented by the spectrum, given the poor angular resolution of the IRAS $100 \mu\text{m}$ maps; and (2) the “isotropic” ISRF strengths derived from the cirrus are likely to be biased low if we are primarily seeing back scattered radiation from preferentially forward scattering grains in clouds that are mostly illuminated on one side by the Galactic disk.

The absence of a detectable scattered $\text{H}\alpha$ emission line in the cirrus spectrum suggests that the radiation incident on the clouds has the spectrum of an early type galaxy, E or Sa. This is understandable if the cirrus is local (heliocentric distance $\lesssim 300 \text{ pc}$), in which case it is illuminated mainly by a part of the disk

between spiral arms (which are separated by roughly 2–3 kpc). The inter-arm region is dominated by stars that are somewhat older than the global average over the Galaxy, the latter including a contribution from young stars in star forming/HII regions. This explanation for the lack of $\text{H}\alpha$ is indirectly corroborated by independent evidence that the cirrus ERE is excited by a UV-poor radiation field (see below). Moreover, the presence of ERE tends to dilute the reflected $\text{H}\alpha$ emission line, if any, in the cirrus spectra. For completeness, we also present the scattered light spectrum for an ambient Sc-type radiation field (dotted line in second panel of Fig. 1); it is a worse fit to the data than scattered light based on an E-type spectrum.

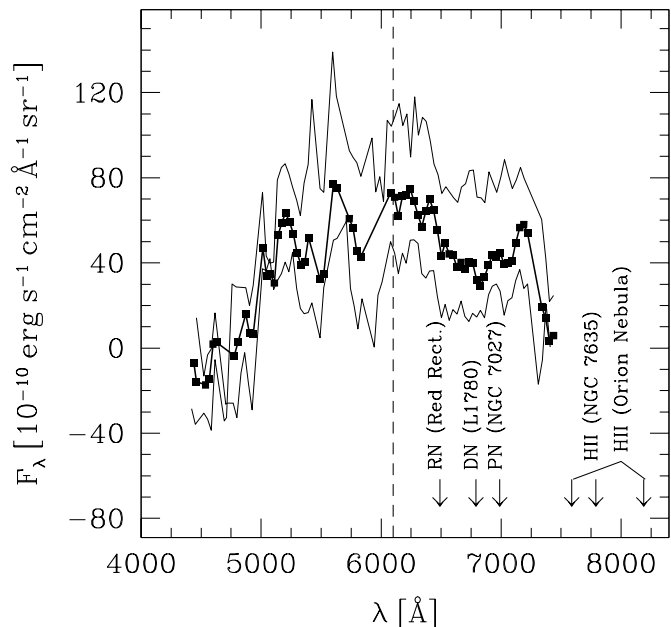


Fig. 2.— The difference between the cirrus spectrum and the best fit (at $\sim 4500 \text{ \AA}$) scattered light model, averaged over the three clouds (bold line) and for LBN 8 and Witch (upper and lower thin solid lines). The dashed vertical line shows the approximate central wavelength of the ERE. The arrows show the peak wavelengths of the ERE in a number of astronomical objects; a reflection nebula (RN), a dark nebula (DN), a planetary nebula (PN) and HII regions.

In Fig. 2 we plot the average difference between the cirrus spectrum and the best fit (at $\sim 4500 \text{ \AA}$)

scattered light model, over the 4000 Å–7500 Å range within which flux measurements are reliable. The thin solid lines indicate the ERE for LBN 8 and Witch, the clouds with the strongest and weakest excess, respectively. These also provide some measure of the uncertainty in our estimate of the average cirrus ERE spectrum.

Furton & Witt (1993) have conducted laboratory experiments on HAC and AC (pure amorphous carbon) films to address astronomical observations of ERE. They find that UV radiation can either diminish or enhance the efficiency of photoluminescence (PL) in hydrogenated carbon solids, depending on the availability of free atomic hydrogen and on the relative H saturation of the solid. UV-annealing and subsequent hydrogenation of HAC dust causes a broadening and shift of the ERE peak towards the red. Furton & Witt note that the observed shifting of the peak ERE emission to longer wavelengths in objects with intense UV radiation, such as HII regions and planetary nebulae, must indeed be a consequence of this. Comparing the shape of the cirrus ERE (Fig. 2) with laboratory PL yield (Fig. 1 of Furton & Witt 1993), we see excellent agreement in both shape and width of the feature. We also indicate in Fig. 2 the approximate central wavelengths λ_0 of the ERE in a number of astronomical objects: the HII regions NGC 7635 (Sivan & Perrin 1993) and the Orion Nebula (Perrin & Sivan 1992), the planetary nebula NGC 7027 (Furton & Witt 1990), the dark nebula L1780 (Mattila 1979; Chlewicki & Laureijs 1987), and the reflection nebula called the “Red Rectangle” around HD 44179 (Schmidt et al. 1980). In agreement with Furton & Witt’s laboratory experiments, the peak of the cirrus ERE, $\lambda_0 \sim 6000$ Å, appears to be located at bluer wavelengths than the ERE emission seen in environments with higher UV radiation.

The integrated ERE intensity of the cirrus is $1.2 \times 10^{-5} \text{ erg s}^{-1} \text{ cm}^{-2} \text{ sr}^{-1}$ and the ratio of ERE to scattered intensity is ~ 0.3 , in good agreement with the findings of Gordon et al. (1997): $I_{\text{ERE}} \approx 10^{-5} \text{ erg s}^{-1} \text{ cm}^{-2} \text{ sr}^{-1}$ and $I_{\text{ERE}}/I_{\text{sca}} = 0.05\text{--}2$ in the diffuse ISM. For other objects $I_{\text{ERE}}/I_{\text{sca}}$ ranges from 0.01–0.68 in reflection nebulae to 0.2–0.6 in HII regions. Applying the same conversions as Gordon et al. (1997), we find the cirrus has an ERE photon efficiency of $\sim 10\%$.

The shape of inferred cirrus ERE spectrum looks remarkably similar to laboratory ERE spectra and to ERE in other astrophysical objects, and there is a perfectly reasonable explanation for the shift of the

cirrus ERE peak to the blue relative to objects with hotter illuminating sources. Nevertheless, the cirrus ERE spectrum derived from this initial study should be treated as preliminary (pending more thorough follow-up observations) in light of the uncertainties in the data and in the scattered light model discussed above.

4. Summary

We present long slit spectra straddling sharp edges in three high latitude Galactic cirrus clouds. The cirrus is clearly detected in each case. The shape of the cirrus spectrum does not match the shape of scattered ambient interstellar radiation, modeled using synthetic galaxy spectra. Assuming the blue end of the cirrus spectrum is dominated by scattered light, there is an excess emission in the range 5000 Å–7000 Å, in good agreement with the Extended Red Emission (ERE) bump seen in other astronomical objects. The integrated ERE intensity ($\sim 10^{-5} \text{ erg s}^{-1} \text{ cm}^{-2} \text{ sr}^{-1}$) and ratio between ERE and scattered light (~ 0.3) agree well with values inferred from color measurements of the diffuse Galactic light (Gordon et al. 1997). The position of the peak ERE emission in cirrus (~ 6000 Å), compared to objects such as HII regions and planetary nebulae, is consistent with a relatively UV-poor ambient radiation field.

The initial phases of this project were supported by a Faculty Research grant at UCSC. AS and PG are supported in part by NASA LTSA grant NAG 5-3232; PG is supported in part by an Alfred P. Sloan Foundation fellowship. It is a pleasure to thank Roc Cutri for help with target selection and other aspects of the cirrus project. We also thank Dan Kelson for help with his Expector spectroscopic analysis program, Karl Gordon for sharing unpublished results, and the referee for useful comments.

REFERENCES

- Beichman, C. A. 1987, *ARA&A*, 25, 521
- Boulanger, F., Baud, B., and van Albada, G. D. 1985, *A&A*, 144, L9
- Boulanger, F., Beichman, C., Desert, F. X., Helou, G., Perault, M., and Ryter, C. 1988, *ApJ*, 332, 328
- Boulanger, F., and Perault, M. 1988, *ApJ*, 330, 964
- Boulanger, F. 1994, in *The First Symposium on the Infrared Cirrus and Diffuse Interstellar Clouds*,

- eds. R. M. Cutri & W. B. Latter (San Francisco: BookCrafters, Inc.), 101
- Burton, M. G., Moorhouse, A., Brand, P. W. J. L., Roche, P. F., and Geballe, T. R. 1988, in Proc. IAU Symp. 135, *Interstellar Dust: Contributed Papers*, eds. L. J. Allamandola and A. G. G. M. Tielens (NASA CP-3036), 87
- Cardelli, J. A., Clayton, G. C., and Mathis, J. S. 1989, *ApJ*, 345, 245
- Chlewicki, G., and Laureijs, R. J. 1987, in *Polycyclic Hydrocarbons and Astrophysics*, eds. A. Léger et al. (Reidel Publishing Company), 335
- d'Hendecourt, L., Léger, A., Olofsson, G., and Schmidt, W. 1986, *A&A*, 170, 91
- de Vaucouleurs, G. 1955, *Observatory*, 75, 129
- de Vaucouleurs, G. 1960, *Observatory*, 80, 106
- de Vries, C. P., and le Poole, R. S. 1985, *A&A*, 145, L7
- Draine, B. T., and Lee, H. M. 1984, *ApJ*, 285, 89
- Duley, W. W. 1985, *MNRAS*, 215, 259
- Duley, W. W., and Williams, D. A. 1988, *MNRAS*, 230, 1P
- Duley, W. W., and Williams, D. A. 1990, *MNRAS*, 247, 647
- Fioc, M., and Rocca-Volmerange, B. 1997, in preparation
- Furton, D. G., and Witt, A. N. 1990, *ApJ*, 364, L45
- Furton, D. G., and Witt, A. N. 1992, *ApJ*, 386, 587
- Furton, D. G., and Witt, A. N. 1993, *ApJ*, 415, L51
- Gordon, K. D., Witt, A. N., and Friedmann, B. C. 1997, in preparation
- Guhathakurta, P., and Tyson, J. A. 1989, *ApJ*, 346, 773
- Guhathakurta, P., and Draine, B. T. 1989, *ApJ*, 345, 230
- Guhathakurta, P., and Cutri, R. M. 1994, in *The First Symposium on the Infrared Cirrus and Diffuse Interstellar Clouds*, eds. R. M. Cutri & W. B. Latter (San Francisco: BookCrafters, Inc.), 34
- Heiles, C. 1975, *A&AS*, 20, 32
- Heiles, C., Reach, W. T., and Koo, B.-C. 1988, *ApJ*, 332, 13
- Low, F. J. et al. 1984, *ApJ*, 278, L19
- Lynds, B. T. 1965, *ApJS*, 12, 163
- Mathis, J. S., Mezger, P. G., and Panagia, N. 1983, *A&A*, 128, 212
- Mattila, K. 1979, *A&A*, 78, 253
- Mezger, P. G., Mathis, J. S., and Panagia, N. 1982, *A&A*, 105, 373
- Osterbrock, D. E., and Martel, A. 1992, *PASP*, 104, 76
- Paley, E. S. 1990, M.S. thesis, University of Arizona
- Paley, E. S., Low, F. J., McGraw, J. T., Cutri, R. M., and Rix, H.-W. 1991, *ApJ*, 376, 335
- Perrin, J.-M., and Sivan, J.-P. 1992, *A&A*, 255, 271
- Perrin, J.-M., Darbon, S., and Sivan, J.-P. 1995, *A&A*, 304, L21
- Poggianti, B. M. 1997, *A&AS*, 122, 399
- Puget, J. L., and Boulanger, F. 1985, *A&A*, 142, L19
- Sandage, A. 1976, *AJ*, 81, 954
- Savage, B. D., and Mathis, J. S. 1979, *ARA&A*, 17, 73
- Schmidt, G. D., Cohen, M., and Margon, B. 1980, *ApJ*, 239, L133
- Scott, A. D., Evans, A., and Rawlings, J. M. C. 1994, *MNRAS*, 269, L21
- Sivan, J.-P., and Perrin, J.-M. 1993, *ApJ*, 404, 258
- Stark, R. 1993, Ph.D. thesis, University of Leiden
- Stark, R. 1995, *A&A*, 301, 873
- Webster, A. 1993, *MNRAS*, 264, L1
- Witt, A. N., and Schild, R. E. 1988, *ApJ*, 325, 837
- Witt, A. N., and Malin, E. P. 1989, *ApJ*, 347, L25